# Palladium nanoparticles supported on manganese oxide–CNT composites for solvent-free aerobic oxidation of alcohols: Tuning the properties of Pd active sites using $MnO_x$

Hui Teng Tan [a], Yuanting Chen [b], Chunmei Zhou [b], Xinli Jia [b], Jixin Zhu [a], Jing Chen [a], Xianhong Rui [a], Qingyu Yan [a,*], Yanhui Yang [b,*]

[a] School of Materials Science and Engineering, Nanyang Technological University, Singapore 639798, Singapore
[b] School of Chemical and Biomedical Engineering, Nanyang Technological University, Singapore 637459, Singapore

## ARTICLE INFO

## ABSTRACT

The manganese oxide-multi-walled carbon nanotube ($MnO_x$/CNT) composite was successfully synthesized following a surface deposition method. Subsequently, the palladium nanoparticles were homogeneously deposited onto this $MnO_x$/CNT hybrid material followed by being reduced under $H_2$ atmosphere. The catalytic activity in solvent-free benzyl alcohol oxidation was correlated with $MnO_x$ loading, indicating the important role of manganese oxide in tuning the properties of Pd catalytic active site, e.g., dispersion and electron density. In the presence of reducible $MnO_x$ on CNT, the electron transfer and oxygen activation were greatly enhanced because of the synergistic interaction between Pd metallic nanoparticles and the hybrid support materials. Due to this strong metal support interaction (SMSI), the Pd/$MnO_x$/CNT catalysts were remarkably stable against deactivation.

© 2012 Elsevier B.V. All rights reserved.

## 1. Introduction

Benzaldehyde is a commercially valuable product in the perfumery, pharmaceutical and flavoring industries. It is also an important chemical building block in research laboratories. Hence, the selective oxidation of benzyl alcohol to benzaldehyde is a widely studied reaction particularly in the field of heterogeneous catalysis [1–3]. In recent year, environmental issue has become a major concern, and in this regard, tremendous effort was devoted to seeking for greener approaches for this reaction. Conventionally, benzyl alcohol oxidation was performed in organic solvents such as toluene, diethoxyethane, dimethylformamide (DMF) and dimethyl sulfoxide (DMSO), which is less environmentally benign due to the presence of hazardous organic wastes [4,5]. In addition, employing base as a promoter [6,7] and stoichiometric amounts of strong oxidizing agents [8] also induce environmental problems. Gas phase oxidation of benzyl alcohol is one of the alternatives although the problem of $CO_2$ greenhouse gas generation remains [9,10]. Therefore, the solvent-free aerobic oxidation of benzyl alcohol using molecular oxygen or air as the oxidant has drawn much attention recently [11–13].

A wide variety of catalysts have been reported for the aerobic oxidation of benzyl alcohol in previous studies [14–16]. In the past decades, palladium catalyst has raised considerable interest because it outperforms other noble-metal-based catalysts in the oxidation of benzyl alcohol [17,18]. Our previous results also showed the superior catalytic properties of surface functionalized TUD-1 supported Pd [19] and Au-Pd/SBA-16 [20] in the solvent-free aerobic oxidation of benzyl alcohol. In the selective oxidation of alcohols over supported palladium catalysts, support materials such as metal oxides [21,22], and carbonaceous materials [23,24] may remarkably influence the catalytic activities. For instance, carbonaceous materials such as carbon nanotubes (CNTs) provide a large surface area and high electronic conductivity to facilitate electron transfer. Metal oxides that are stable in the strongly oxidizing environment prevent agglomeration of the supported metallic nanoparticles due to its strong synergistic effect [25]. Furthermore, reducible metal oxides ($MnO_x$, $CeO_x$, $VO_x$, $TiO_x$) are frequently employed as supports due to their superior oxygen spillover capability [26,27]. In this contribution, manganese oxide–CNT hybrid support materials ($MnO_x$/CNT) were synthesized to combine the advantages of both support materials via a facile depositing method [28]. To examine the catalytic activity of Pd metallic nanoparticles supported on these synthesized nano-composites, the selective oxidation of alcohols, primarily benzyl alcohol using molecular oxygen was employed as a probe reaction.

* Corresponding authors. Tel.: +65 6316 8940; fax: +65 6794 7553.
E-mail addresses: alexyan@ntu.edu.sg (Q. Yan), yhyang@ntu.edu.sg (Y. Yang).

## 2. Experimental

### 2.1. Chemicals

Manganese acetylacetonate ($Mn(C_5H_8O_2)_2$, >97%, Sigma–Aldrich), palladium chloride ($PdCl_2$, 99%, Aldrich), nitric acid ($HNO_3$, 68%, Sigma–Aldrich), Nafion solution (5% in ethanol and water, Sigma–Aldrich), benzyl alcohol (>99%, Sigma–Aldrich), tetradecane (>99.5%, Fluka), ethanol (>99.5%, Sigma–Aldrich), ethyl acetate (>99.5%, Acros), anhydrous toluene (>99.9%, Sigma–Aldrich) were used as received without any further purification.

### 2.2. Synthesis

Commercially available CNTs powder (>95%, Cnano) was treated in concentrated nitric acid to remove impurities and create oxygen-containing groups on CNT surfaces: a mixture of CNTs powder (2 g) and concentrated nitric acid (100 mL) was refluxed at 120 °C for 4 h. Subsequently, the acid-treated CNTs was filtered and washed with deionized water for several times before drying at 60 °C overnight. The procedure for depositing manganese oxide onto functionalized CNTs is as follows: 0.5 g of functionalized CNTs and a certain amount of manganese (II) acetylacetonate ($Mn(C_5H_8O_2)_2$) were suspended in 50 mL of anhydrous toluene separately and refluxed at 110 °C for 5 h under inert nitrogen atmosphere to remove moisture. These two suspensions were mixed together and refluxed at 110 °C for another 12 h to deposit manganese onto the surface of CNTs. The suspension was filtered and dried overnight followed by annealing at 400 °C for 6 h under a nitrogen flow. The obtained composite material was denoted as $x$MnO$_x$/CNT where $x$ refers to Mn loadings (0–10 wt.%). Wetness impregnation was employed to deposit palladium precursors onto MnO$_x$/CNT hybrid support: 379.7 μL of PdCl$_2$·2HCl (0.05 M) was added dropwise into 20 mL of aqueous suspension pre-charged with 0.2 g of MnO$_x$/CNT and the mixture was stirred at 80 °C for 5 h. The suspension was filtered, washed with deionized water and dried overnight. After reducing in the H$_2$ flow at 400 °C for 2 h, the obtained catalysts were denoted as Pd/$x$MnO$_x$/CNT.

### 2.3. Characterizations

Powder X-ray diffraction (XRD) was performed on Bruker AXS D8 Advance diffractometer with Cu K$\alpha$ radiation ($\lambda = 0.15406$ nm). The diffraction pattern was collected within 20–60° ($2\theta$). Inductively coupled plasma (ICP, Dual-view Optima 5300 DV ICP-OES system) was employed to measure the elemental contents of Pd/$x$MnO$_x$/CNT. Concentrated hydrofluoric acid (40%) was used to digest the samples prior to the measurements. The instrument used in transmission electron microscopy (TEM) was JOEL JEM 2100F, operating at 200 kV. X-ray photoelectron spectroscopy (XPS) measurements were performed on VG Escalab 250 spectrometer using Al K$\alpha$ 1846.6 eV anode. The binding energy was calibrated using C 1$s$ peak at 284.6 eV as the reference.

The electrochemical characterizations were carried out on Autolab PGSTAT302 potentiostat. A three-electrode system consisting of Ag/AgCl reference electrode, Pt wire counter electrode and glassy carbon working electrode was employed in cyclic voltammetry (CV) and rotating disk electrode (RDE) voltammetry. The catalyst ink was prepared by mixing 3 mg of Pd/$x$MnO$_x$/CNT catalyst with 0.75 mL of ethanol and 0.75 mL of Nafion solution (0.05%). For CV measurement, the working electrode was coated with 50 μL of catalyst ink. The cyclic voltammograms were scanned in a 1 M of NaOH solution under saturated N$_2$ condition with 50 mV s$^{-1}$ scan rate. The RDE voltammetry to measure the oxygen reduction was carried out in 1 M of NaOH solution under O$_2$ saturated condition with 10 mV s$^{-1}$ scan rate and 1600 rpm rotating speed.

### 2.4. Oxidation of benzyl alcohol

The catalytic reaction was performed under solvent-free conditions. Benzyl alcohol (5.174 mL, 50 mmol) and catalyst (5 mg) were loaded in a 25 mL three-necked round bottom flask. Prior to the oxidation of benzyl alcohol, the reaction mixture was purged with argon for 1 h to eliminate the trapped residual air. The mixture was then immersed in a 160 °C oil bath and the oxygen (flow rate: 20 mL min$^{-1}$) was bubbled into the mixture to initiate the reaction. The reaction was run for 1 h under vigorous stirring (stirring rate: 1200 rpm). The liquid products were collected and analyzed by Agilent gas chromatograph 6890 equipped with a HP-5 capillary column. Dodecane was the internal standard to quantify the concentration of remaining reactant and products formed. The conversion, selectivity and *quasi*-turnover frequency (*q*TOF) are defined as follows:

$$\text{Conversion} \ (\%) = \frac{\text{Moles of reactant converted}}{\text{Moles of reactant in feed}} \times 100\%$$

$$\text{Selectivity} \ (\%) = \frac{\text{Moles of product formed}}{\text{Moles of reactant converted}} \times 100\%$$

$$q\text{TOF} \ (\text{h}^{-1}) = \frac{\text{Moles of reactant converted}}{\text{Moles of total active sites} \times \text{reaction time}}$$

## 3. Results and discussion

### 3.1. Characterizations of as-synthesized catalysts

As shown in Fig. 1a, the diffraction peaks at 26° and 43° can be indexed to the (0 0 2) and (1 0 0) planes of graphitic CNT, respectively [29]. The diffraction peak at 41° shown in Pd/CNT is accord with (1 1 1) plane of metallic Pd [30]. It is worth noting that the Pd (1 1 1) diffraction peak becomes less distinct in the presence of manganese oxide. This phenomenon is a good indication to reveal the structural or electronic changes of Pd catalytic active site that can be due to several reasons: (1) particle size of Pd is smaller; (2) the degree of crystallinity of Pd nanoparticle decreases; (3) the lattice $d$-spacing of Pd deviates from the reference. From the TEM images and Pd nanoparticle size distribution histogram, constructed by calculating ca. 200 Pd nanoparticles of the as-synthesized catalysts shown in Fig. 2, the particle size effect can be ruled out, as the Pd particles are not perceived to be smaller in size. The average Pd particle sizes of Pd/CNT, Pd/2.5MnO$_x$/CNT and Pd/10MnO$_x$/CNT were 3.6, 3.9, and 4.0 nm respectively. Likewise, the HRTEM images confirmed the well-crystallined Pd nanoparticles of these as-synthesized samples. Hence, we attributed the change in Pd (1 1 1) diffraction peak intensity to the change in lattice $d$-spacing which is largely accounted for the SMSI [31].

The XRD diffraction peaks for MnO$_x$ are hardly to be detected, indicating the characteristics of homogeneous dispersion of MnO$_x$ over the surfaces of CNT. Furthermore, the crystal structure of manganese species was also investigated using HRTEM. In Fig. 2c and e inset, highly dispersed manganese oxides showing the lattice $d$-spacing of 2.72 Å (JCPDS 041-1442) on CNT surfaces can be clearly seen, which are closely contacted with Pd nanoparticles. The deposition method employed in this study has been proved to be effective to homogeneously deposit metal precursor on CNT surfaces. The cationic metal precursor is chemically attached to the functionalized CNT using the oxygen-containing groups as anchoring sites. Hence, manganese oxide is uniformly deposited while the particle size is well-controlled to nano-dimensions [28].
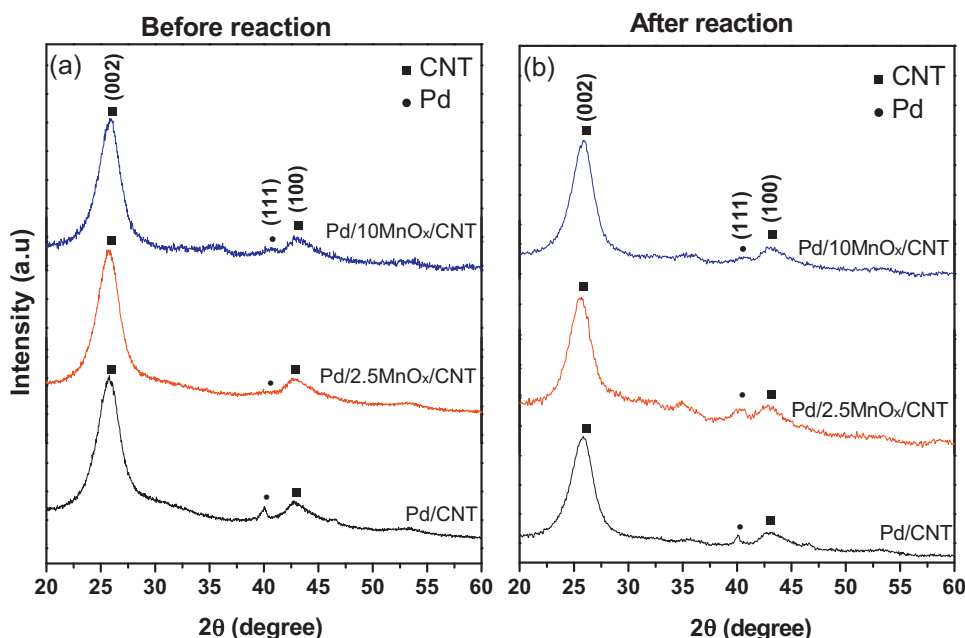
**Before reaction**

**After reaction**



Fig. 1. XRD diffraction patterns of Pd/xMnO$_x$/CNT.

The XPS core level spectra of Pd 3$d$, Mn 2$p$ and O 1$s$ were investigated and the deconvoluted XPS spectra are shown in Fig. 3. The calculated abundance of different surface species is also summarized in Table 1. The Pd 3$d$ peaks can be deconvoluted to 2 oxidation states, indicating the co-existence of Pd metallic state and Pd$^{2+}$ cationic state in the as-synthesized catalysts. The fraction of Pd$^{2+}$ increases in the presence of manganese oxide. With the deposition of nano-sized manganese oxide on CNT surfaces, the electron transfer between the intimately contacted Pd and mixed-valence MnO$_x$ cluster will be enhanced due to the reduction–oxidation chemistry. From this point of view, the electrons inherently should flow from MnO$_x$ to the electron deficient Pd site [32,33]. However, upon loading higher amounts of manganese precursor, a larger extent of contact between manganese oxides and Pd nanoparticles is expected after pre-reduction in hydrogen. The electronic interaction that occurs at the interfacial region of Pd and MnO$_x$ may stabilize Pd$^{2+}$ species at higher oxidation state.

Even though the existence of mixed valence MnO$_x$ (Mn$^{3+}$, Mn$^{3+}$, Mn$^{4+}$) species cannot be characterized using XRD, the non-stoichiometric MnO$_x$ transition metal oxide exhibits multiple oxidation states in XPS elemental analysis. In XPS analysis, the Mn 2$p_{3/2}$ peak can be resolved into Mn$^{4+}$ (642.8 eV) and Mn$^{3+}$ (641.5 eV). A remarkable increase in the amount of Mn$^{4+}$ as the manganese loading increases can be explained by SMSI. The SMSI is referred to the mutual electronic interaction between metal and oxides support: Pd changes the oxidation state of MnO$_x$ and MnO$_x$

also tunes the electronic structure of Pd [33]. As mentioned previously, the high valence state Mn$^{4+}$ found in Pd/10MnO$_x$/CNT is due to the large extent contact for electron transfer upon increasing the amount of manganese species. Inversely, this effect is less pronounced in Pd/2.5MnO$_x$/CNT that stabilizes the high valence Mn$^{4+}$ from being reduced. The deconvoluted O 1$s$ peaks show several types of oxygen species: the binding energy of lattice oxygen (O$_2$$^{2-}$) falls between 529.8 and 530.1 eV, the binding energy of C=O and C−O on CNT surfaces are ascribed as 531–532 eV and 532–533 eV, respectively [34]. The highest binding energy in the range of 534–536 eV is most likely due to the chemisorbed oxygen or adsorbed molecular H$_2$O [35]. Therefore, the electronic interaction between Pd active sites and MnO$_x$ was manifested here. Higher abundance of high oxidation state of ionic manganese species can accommodate more mobile lattice oxygen to form greater amount of Mn$^{x+}$−O$^{2-}$ Lewis acid-base pair [36]. Thus, one can observe that the concentration of lattice oxygen increases with the manganese loading.

### 3.2. Electrochemical characterization of Pd/MnO$_x$/CNT catalyst

Our previous studies showed that the oxygen activation were remarkably enhanced in the aqueous phase benzyl alcohol oxidation over a FeO$_x$/Pt/CNT catalyst due to the presence of ferrous oxide [37]. In this study, electrochemical measurements were carried out to characterize the electronic interaction in these Pd/MnO$_x$/CNT

**Table 1**
Surface composition in XPS analysis of as-synthesized catalysts.[a,b]

| Catalyst | Surface composition (%) | | | | | | | |
|---|---|---|---|---|---|---|---|---|
| | Pd$^0$/Pd | | Pd$^{2+}$/Pd | | Mn$^{3+}$/Mn | | Mn$^{4+}$/Mn | |
| | Before[c] | After[d] | Before[c] | After[d] | Before[c] | After[d] | Before[c] | After[d] |
| Pd/CNT | 53.3 | 57.4 | 46.7 | 42.6 | – | – | – | – |
| Pd/2.5MnO$_x$/CNT | 52.2 | 60.2 | 47.8 | 39.8 | 53.1 | 45.1 | 46.9 | 54.9 |
| Pd/10.0MnO$_x$/CNT | 32.9 | 50.3 | 67.1 | 49.7 | 32.0 | 22.3 | 68.0 | 77.7 |

[a] The concentration of palladium species (Pd$^0$ and Pd$^{2+}$) was derived from the deconvoluted Pd 3$d_{5/2}$ XPS peak.

[b] The concentration of manganese species (Mn$^{2+}$, Mn$^{3+}$, Mn$^{4+}$) was derived from the deconvoluted Mn 2$p_{3/2}$ XPS peak.

[c] The surface composition was calculated from the fresh catalysts before the oxidation reaction.

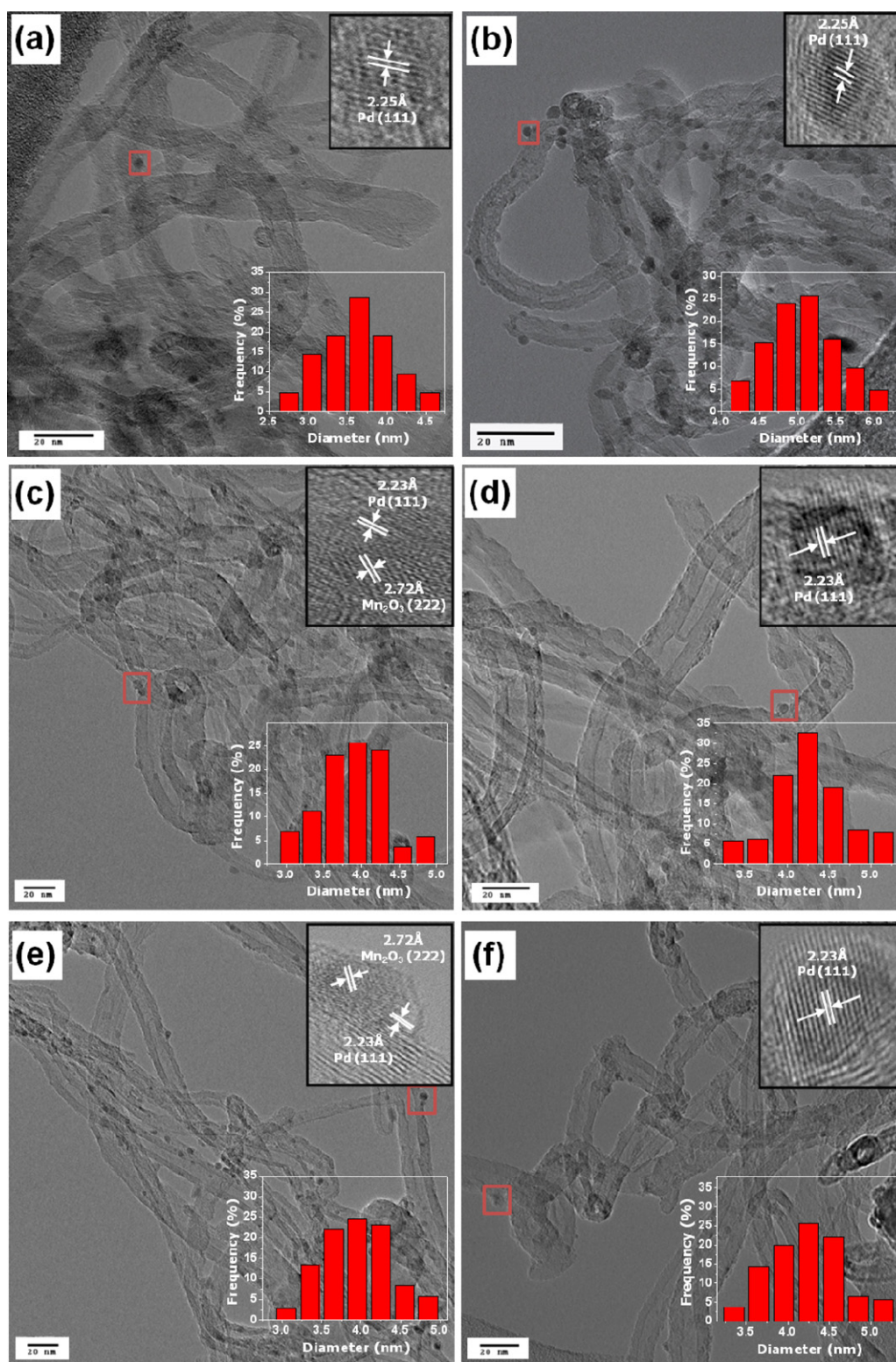[d] The surface composition was calculated from the catalysts after the oxidation reaction.

**Fig. 2.** TEM images and Pd size distribution histograms before and after reaction. Before: (a) Pd/CNT; (c) Pd/2.5MnO$_x$/CNT; (e) Pd/10MnO$_x$/CNT. After: (b) Pd/CNT; (d) Pd/2.5MnO$_x$/CNT; (f) Pd/10MnO$_x$/CNT.

samples. Fig. 4a shows the CV curves in the alkaline medium under saturated N$_2$ condition. The amount of electrons involved can be calculated by integrating the enclosed area of CV curve, which reflects the electron transfer efficiency in the redox reaction [38]. The results indicate that the electronic interaction is significantly enhanced after loading manganese oxides. The reduction potentials of Pd$^{2+}$ shift negatively as shown in Fig. 4b, suggesting that

the reduction of Pd$^{2+}$ in Pd/MnO$_x$/CNT becomes more difficult and more Pd species remain in cationic state compared to Pd/CNT, which is consistent with the results in Pd 3$d$ XPS analysis. The RDE polarization voltammetry to investigate the oxygen reduction reaction (ORR) was conducted under O$_2$ saturated conditions and the results are shown in Fig. 5. These as-synthesized catalysts showed almost identical onset of O$_2$ reduction potential that
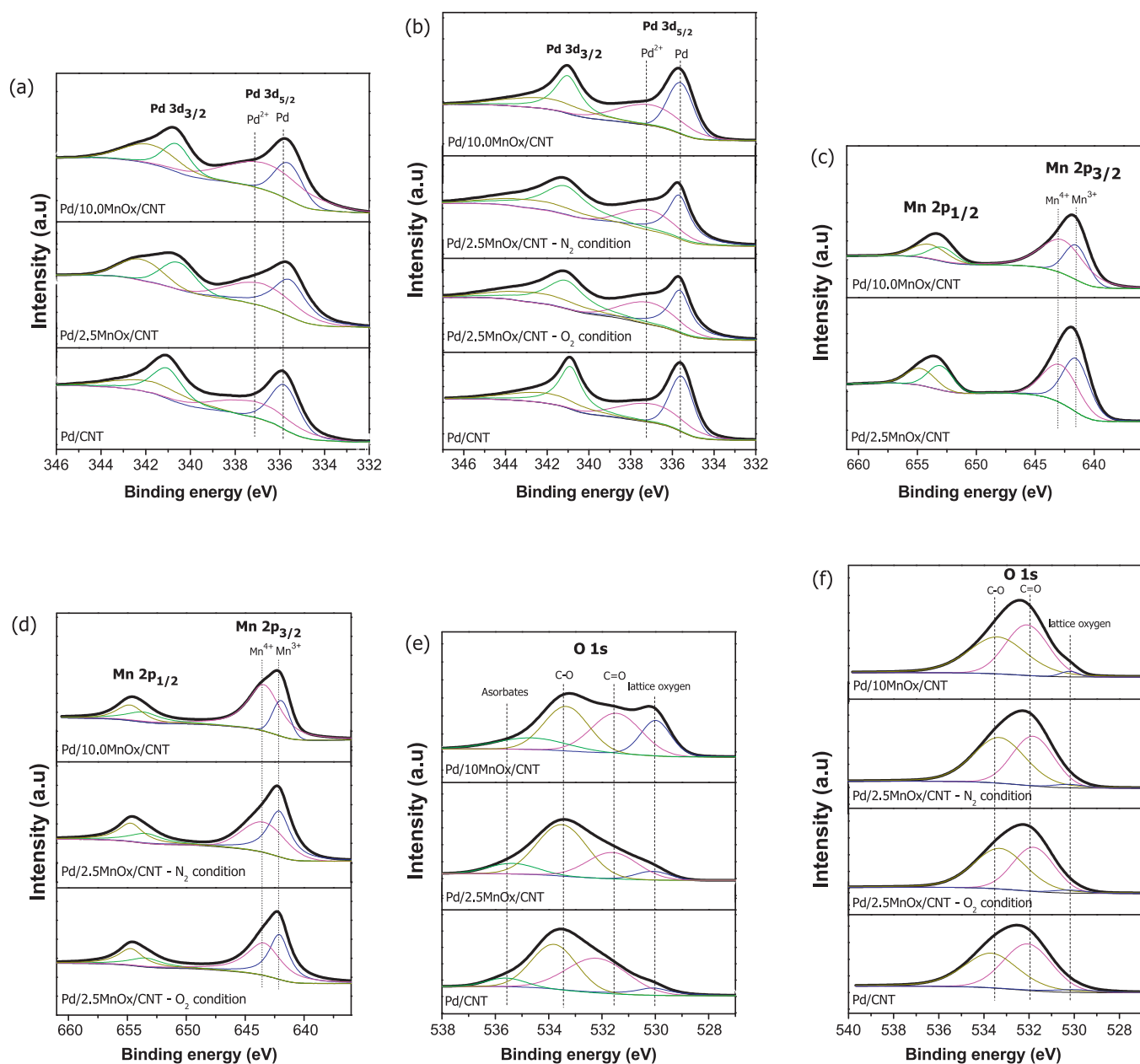
**Fig. 3.** XPS spectra, (a, b) Pd 3*d* spectra before and after reaction respectively; (c, d) Mn 2*p* spectra before and after reaction respectively; (e, f) O 1*s* spectra before and after reaction respectively.

occurs at $-0.06$ V in alkaline medium. The inset in Fig. 5 shows a linear relationship between the manganese loading and the steady-state diffusion current corresponding to $O_2$ reduction, showing that the ORR electro-catalytic activities is sensitive to manganese loading. In this study, $Pd/10MnO_x/CNT$ outperforms $Pd/CNT$ and $Pd/2.5MnO_x/CNT$, showing the highest current density over a large potential range ($\sim$0.45 V). The enhancement in oxygen reduction can be correlated to the promotion of oxygen activation at higher abundance of high oxidation state manganese oxide species that facilitate the transformation of atmospheric oxygen to the lattice oxygen, and subsequently migration of lattice oxygen to Pd active sites [39].

### 3.3. Catalytic activity of $Pd/MnO_x/CNT$ catalyst

The catalytic activities of $Pd/MnO_x/CNT$ were evaluated in the aerobic oxidation of benzyl alcohol and the results are summarized in Table 2. All the catalysts show high selectivities toward benzalde-hyde as the desired product within the allowed reaction duration. Incorporation of a moderate amount of $MnO_x$ remarkably improves the catalytic activity, whereas $Pd/10MnO_x/CNT$ shows the poorest conversion. The experiments were also conducted under anaerobic atmosphere using $N_2$ instead of $O_2$. All the as-synthesized catalysts showed almost zero conversion and $q$TOF, indicating the important role of molecular $O_2$ as the oxidant to oxidize and remove adsorbed species on the catalytic active site and regenerate the fresh surfaces for next catalytic cycle [40].

Fig. 6 shows the time course activities of representative catalysts in benzyl alcohol oxidation. The order of initial rate is $Pd/2.5MnO_x/CNT > Pd/CNT > Pd/10MnO_x/CNT$. $2.5MnO_x/CNT$ without Pd shows almost zero conversion, indicating that Pd is the primary catalytically active site toward the oxidation of benzyl alcohol. All the catalysts show a gradual decay in catalytic activity ($q$TOF) and this deactivation is a result of either the coverage of

**Table 2**
The catalytic performance of Pd/xMnO$_x$/CNT catalysts.[a]

| Catalysts | Metal content[b] (wt.%) | | Conversion (%) | | Selectivity (%) | | | | | | qTOF[c] (h$^{-1}$) | |
|---|---|---|---|---|---|---|---|---|---|---|---|---|
| | | | | | Toluene | | Benzylaldehyde | | Benzoic acid | | | |
| | | | N$_2$ | O$_2$ | N$_2$ | O$_2$ | N$_2$ | O$_2$ | N$_2$ | O$_2$ | N$_2$ | O$_2$ |
| Pd/CNT | Pd | 0.88 | 0.3 | 12.5 | 0 | 0 | 100 | 100 | 0 | 0 | 419 | 15118 |
| Pd/2.5MnO$_x$/CNT | Pd | 0.84 | 1.8 | 15.4 | 0 | 0 | 100 | 100 | 0 | 0 | 2329 | 19467 |
| | Mn | 1.08 | | | | | | | | | | |
| Pd/5.0MnO$_x$/CNT | Pd | 0.85 | 1.0 | 14.6 | 0 | 0 | 100 | 100 | 0 | 0 | 1314 | 18232 |
| | Mn | 3.00 | | | | | | | | | | |
| Pd/7.5MnO$_x$/CNT | Pd | 0.86 | 0.9 | 12.2 | 0 | 0 | 100 | 100 | 0 | 0 | 1101 | 15121 |
| | Mn | 5.02 | | | | | | | | | | |
| Pd/10.0MnO$_x$/CNT | Pd | 0.81 | 0.7 | 10.6 | 0 | 0 | 100 | 100 | 0 | 0 | 894 | 13937 |
| | Mn | 7.13 | | | | | | | | | | |

[a] Reaction conditions: catalyst, 5 mg; benzyl alcohol, 50 mmol; O$_2$, 20 mL min$^{-1}$; temperature, 160 °C; time, 1 h; experimental error, ±5%.
[b] Metal content was tested by ICP.
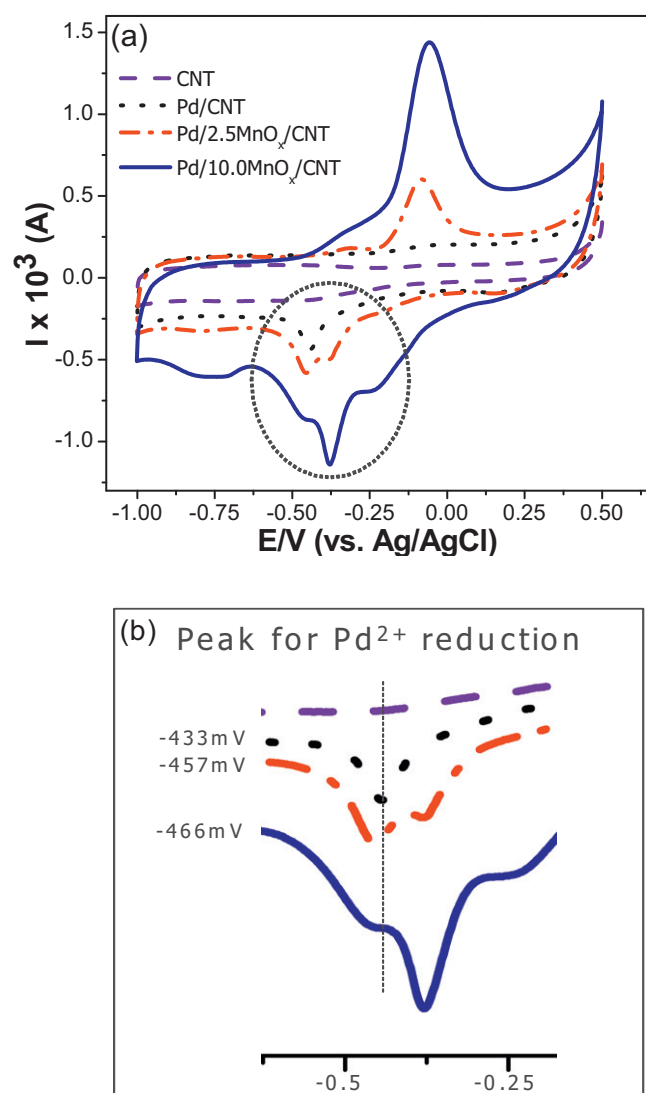[c] qTOF was derived from the Pd metal content tested by ICP.



**Fig. 4.** (a) Cyclic voltammetry of Pd/xMnO$_x$/CNT in 1 M KOH solution under saturated N$_2$ condition; (b) magnification of the circled region that representing the reduction potential of Pd$^{2+}$.

strongly adsorbed species on the surface of Pd nanoparticles [41] or the agglomeration of Pd nanoparticles due to over-oxidation [42]. The coverage of hydrocarbon on the Pd catalytic active site inhibits the adsorption of reactants while the over-oxidation may induce the formation of Pd—O—Pd intermediate, leading to a larger cluster dimension. However, Pd/10MnO$_x$/CNT shows different activity evolution trend from other two catalysts. Initially, Pd/10MnO$_x$/CNT exhibits lower conversion and qTOF owing to the higher concentration of MnO$_x$-stabilized Pd$^{2+}$ (shown in Table 1), which has been regarded to be inactive species in this particular reaction [43]. It is interesting to observe that the conversion of Pd/10MnO$_x$/CNT becomes higher than that of Pd/CNT after approximately 5 h of reaction time. We correlate such catalyst activation period to the valence transition of Pd upon adsorption of alcohol species. During this induction period, the adsorbed alcohol species act as a reducing agent to chemically transform Pd$^{2+}$ into Pd$^0$ phase [44]. Subsequently, the qTOF reaches a plateau after a slight increase in the first few hours, indicating that the Pd nanoparticles in this particular catalyst are more resistant to surface passivation and more stable against agglomeration.
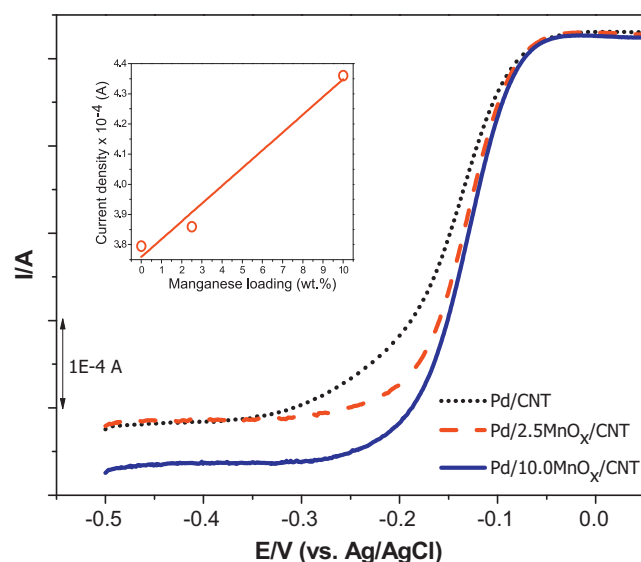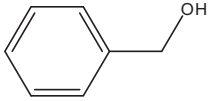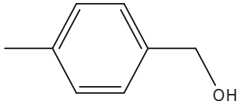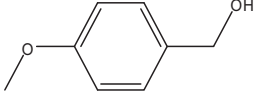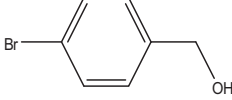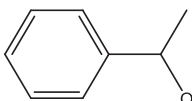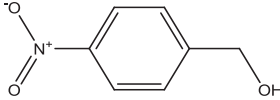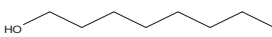


**Fig. 5.** ORR polarization curves of Pd/xMnO$_x$/CNT in 1 M KOH solution with 1600 rpm rotating speed and scan rate of 10 mV s$^{-1}$ under room temperature. Inset: the correlations between the manganese loading and the O$_2$ reduction current density.

**Table 3**
Oxidation of various alcohols using Pd/2.5MnO$_x$/CNT catalyst.[a]

| Entry | Substrate | Time (h) | Conversion (%) | Selectivity[b] (%) | $q$TOF (h$^{-1}$) |
|---|---|---|---|---|---|
| 1 | benzyl alcohol | 1 | 15.4 | 100.0 | 19467 |
| 2 | 4-methylbenzyl alcohol | 1 | 3.2 | 100.0 | 4085 |
|   |   | 3 | 22.5 | 100.0 | 3167 |
|   |   | 6 | 33.5 | 100.0 | 1178 |
| 3 | 4-methoxybenzyl alcohol | 1 | 15.9 | 100.0 | 20169 |
|   |   | 3 | 42.5 | 100.0 | 5977 |
|   |   | 6 | 63.1 | 100.0 | 2221 |
| 4 | 4-bromobenzyl alcohol | 1 | 0.3 | 100.0 | 342 |
|   |   | 3 | 1.9 | 100.0 | 261 |
|   |   | 6 | 7.9 | 100.0 | 276 |
| 5 | 1-phenylethanol | 1 | 17.3 | 100.0 | 21981 |
|   |   | 3 | 21.6 | 100.0 | 3046 |
|   |   | 6 | 24.8 | 100.0 | 874 |
| 6 | 4-nitrobenzyl alcohol | 1 | 0.3 | 100.0 | 320 |
|   |   | 3 | 0.5 | 100.0 | 65 |
|   |   | 6 | 1.4 | 100.0 | 50 |
| 7 | 1-octanol | 1 | 1.4 | 100.0 | 1779 |
|   |   | 3 | 5.0 | 100.0 | 708 |
|   |   | 6 | 19.9 | 100.0 | 699 |

[a] Reaction conditions: catalyst, 5 mg; benzyl alcohol, 50 mmol; O$_2$, 20 mL min$^{-1}$; temperature, 160 °C; experimental error, ±5%.
[b] Selectivity refers to the corresponding aldehyde or ketone.

The oxidation of various alcohol substrates was carried out to investigate the generality of Pd/MnO$_x$/CNT catalyst (represented by Pd/2.5MnO$_x$/CNT) and the results are summarized in Table 3. In general, the activities of Pd/2.5MnO$_x$/CNT in the oxidation of aromatic alcohols with electro-withdrawing group such as 4-methoxybenzyl alcohol, 4-bromobenzyl alcohol and 4-nitrobenzyl alcohol are low. In contrast, the catalytic activity is relatively higher in oxidation of aromatic alcohols with electro-donating group such as 4-methylbenzyl alcohol and 1-phenylethanol and aliphatic alcohol such as 1-octanol. The discrepancy in reactivity can be correlated to the transient formation of the benzylic carbocation intermediate which can be stabilized by the aromatic backbone with electro-withdrawing property upon adsorbing on the catalytic active site to form the metal-alkoxide species [3]. Hence, it confirms that the reaction mechanism is an oxidative dehydrogenation of benzyl alcohol that will be discussed more in depth.

### 3.4. Characterizations of spent catalysts

The spent catalysts show similar XRD diffraction patterns compared to the fresh ones (Fig. 1b). Nevertheless, the XRD peak intensity of Pd increases slightly for used catalysts, indicating the increase in their particle sizes after the reaction, which was further proved by TEM observations. In Fig. 2, the size distribution histograms clearly demonstrate a variation in their particle size of spent catalysts. In the cases of Pd/CNT and Pd/2.5MnO$_x$/CNT, the average particle size increases notably. Undoubtedly, it was a consequence of poor catalytic stability in preventing agglomeration. The average particle size of Pd/10MnO$_x$/CNT remains almost the same as before undergoing the catalytic reaction, suggesting the strong interaction between Pd nanoparticles and MnO$_x$–CNT composite support.

The amounts of Pd$^0$ species increase for these three catalysts after the oxidation reaction which is shown in Table 1. It is believed that Pd requires a transition period, chemically transforming from Pd$^{2+}$ to Pd$^0$ active species to exhibit catalytic capability during this activation period. After 1 h of reaction, Mn$^{4+}$ becomes the dominant species in both Pd/2.5MnO$_x$/CNT and Pd/10MnO$_x$/CNT catalysts, indicating that electrons transfer to the Pd active site and causes MnO$_x$ species to maintain at a high–valence oxidation state. Nonetheless, the change in Mn and Pd oxidation states could be the result of direct interaction with oxygen and alcohol in the
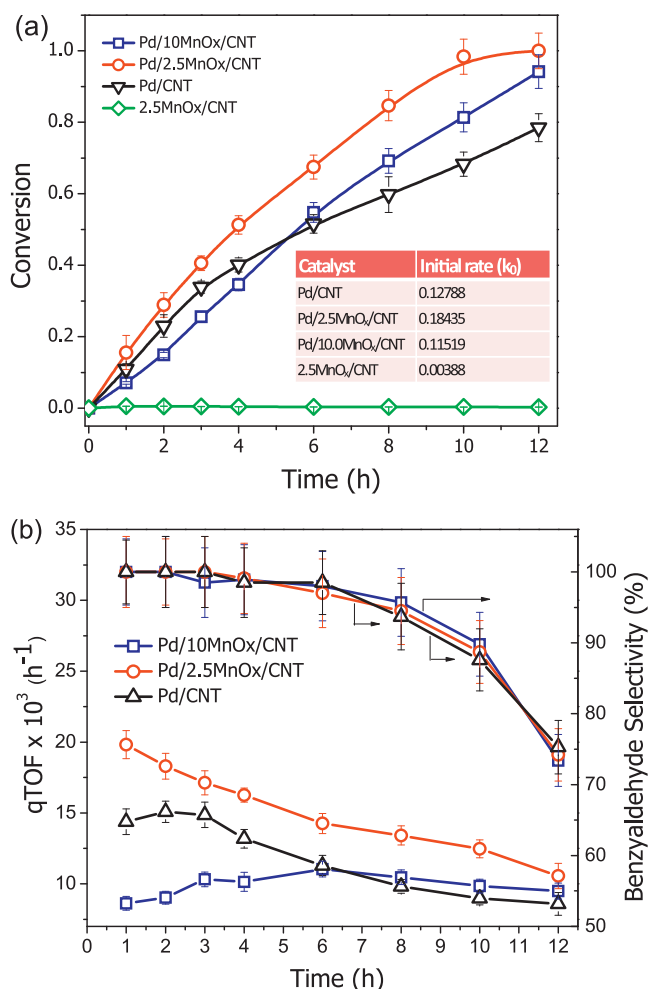
**Fig. 6.** The conversion (a) and $q$TOF (b) as a function of time. Reaction conditions: catalyst, 5 mg; benzyl alcohol, 50 mmol; temperature, 160 °C; time, 12 h.

reaction mixture. To address this issue, in the control experiment, the oxidation reaction was carried out under $N_2$ inert condition, the oxidation states of Pd and Mn were measured by XPS and the results are shown in Fig. 3. The Pd and Mn oxidation states performed under $O_2$ and $N_2$ conditions are similar, implying that oxygen has less effect on inducing the change in oxidation states of Pd and Mn. Likewise, the amount of lattice oxygen in three catalysts shows a decreasing trend after the catalytic reaction, comparing Fig. 3e and f. The depletion of lattice oxygen indicates the migration of lattice oxygen from $MnO_x$ oxygen reservoir to Pd active site to participate in the oxidation reaction.

## 4. Discussion

The experimental results revealed that adding $MnO_x$ to CNT as the support is advantageous in improving the reactivity of Pd/CNT catalysts. The characterization results extracted from XRD and TEM showed the change in lattices constant of Pd nanoparticles after depositing $MnO_x$ onto CNT surfaces. The electrochemical measurements have proved that $MnO_x$ is able to facilitate the electronic interaction, which can be attributed to the consequence of SMSI. Previous studies have shown that the encapsulation of noble metals (Pt, Pd, and Rh) by reducible metal oxides (titanium, vanadium, and manganese) under reducing environment may induce a change in the chemisorption and electronic properties of the metallic active sites [45,46]. Along this line, we attributed the catalytic results to the close contact between Pd

nanoparticles and manganese oxides in the annealing process at 400 °C under $H_2$ flow. The synergistic interaction may perturb the bonding interaction between Pd active sites and the adsorbed species and subsequently change the catalytic properties. Nonetheless, we have found that the manganese loading is an essential parameter in tuning the catalytic performance of the catalysts. As depicted in Table 2, the catalyst only shows superior performance at a rather low concentration of manganese oxide (Pd/2.5MnO$_x$/CNT), where reverse effect emerges at higher manganese loading (Pd/10MnO$_x$/CNT).

Although the $Pd^0$ active species concentration of Pd/2.5MnO$_x$/CNT catalyst is not the highest in the presence of stabilization effect inducing by $MnO_x$, it still surpasses the others which can be reflected by the increments in $q$TOF and conversion. In this context, Pd/2.5MnO$_x$/CNT catalyst shows the best catalytic performance by achieving a good balance between the electronic effect and the oxygen spillover effect. The concentration of $Pd^0$ in Pd/2.5MnO$_x$/CNT catalyst is comparable to Pd/CNT, 52.2% and 53.2% respectively. Nevertheless, the $MnO_x$ support that acts as the oxygen reservoir possess stronger capability in activating molecular oxygen from external system which is confirmed from the RDE polarization voltammetry. Thus, we attributed the further enhancement in the catalytic performance of Pd/2.5MnO$_x$/CNT catalyst compared to Pd/CNT is due to the influence of facile oxygen spillover within the lattice of $MnO_x$. However, after increasing the manganese loading, the catalytic activity of Pd/10MnO$_x$/CNT significantly decreases due to the presence of a large amount of $Pd^{2+}$ inactive species. In addition to the XPS analysis, the negatively shifted reduction potential of $Pd^{2+}$ observed in CV is a good evidence to support the fact that the reducible $MnO_x$ species at higher oxidation states can stabilize the cationic $Pd^{2+}$ (considering the concentration of $Mn^{4+}$ listed in Table 1). The electronic interaction is counted to be the crucial factor for this observation because $MnO_x$ that has been recognized as an oxidation catalyst due to the redox couple of different manganese valences can induce the reduction–oxidation chemistry via facile electron transfer reaction at the interfacial region [47]. Hence, it is not surprising to observe a sharp increase in $Pd^{2+}$ concentration in high manganese loading catalyst. Furthermore, increasing the amount of manganese loading inevitably results in the encapsulation of Pd nanoparticles and eventually suppresses the adsorption of reactants on the Pd active sites, affecting the catalytic activity.

Pd/10MnO$_x$/CNT shows inferior catalytic activity in this study, nonetheless, it has higher stability to withstand the deactivation, which has been proved in the time course experiment. To explain this phenomenon, lattice oxygen of $MnO_x$ species need to be taken into consideration. Previously, Santos and co-workers reported that the lattice oxygen plays an important role in the reactivity of $MnO_x$. According to the Mars van Krevelen mechanism, the oxygen vacancy will be created when the lattice oxygen provided by reducible metal oxides is transported to the catalytic active site and they will be replenished by gaseous molecular oxygen. Implicit in the XPS result is that the catalytic activity of the catalyst is dependent on the chemical state of the manganese species [48]. With higher oxidation state, the manganese species show greater oxygen storage capacity within the lattice [49] and more oxygen vacancies will be created, so the oxygen chemisorption on $MnO_x$ surfaces becomes more favorable. As a result, plenty oxygen diffuses from $MnO_x$ to the vicinity of Pd active sites to get involved in the oxidation of adsorbed species [14,50]. In this study, Pd/10MnO$_x$/CNT catalyst with the largest abundance of lattice oxygen which has been shown in O 1$s$ XPS spectrum can remarkably accelerate the oxidative removal of hydrogen and hydrocarbon species from the Pd catalytic sites due to the enhanced oxygen transfer. For the other two catalysts, the oxygen spillover is not rapid enough to keep pace with the oxidation reaction to regenerate the fresh catalytic

surfaces, deactivation of the catalyst occurs, leading to poor long-term catalytic stability.

## 5. Conclusions

In this study, homogenously dispersed $MnO_x$ on CNT support was successfully synthesized. In addition, coupling the $MnO_x$/CNT hybrid nanocomposite with Pd nanoparticles could be a promising approach to provide improvement in the catalytic activity for benzyl alcohol oxidation and the level of content of manganese oxide in the catalyst plays a critical role by: (1) facilitating the electron transfer at the interfacial region of Pd and $MnO_x$, which changes the physical and chemical properties of the catalyst due to the perturbation of electronic structure of the active sites; (2) promoting oxygen activation by transporting lattice oxygen to Pd catalytic active site. During the catalytic reaction, the oxygen vacancies within $MnO_x$ clusters can be created and replenished by molecular oxygen due to the highly reducible nature of transition metal oxide. Manganese oxide also plays a crucial role in stabilizing $Pd^{2+}$ ionic species. Thus, the reactivity is not linearly dependent of the loading of manganese oxide. In conclusion, we illustrated the important roles of nano-sized manganese oxide support in oxidation of benzyl alcohol and the concept of using metal–metal oxide–carbon system may potentially be applied to other heterogeneous catalytic reactions.

## Acknowledgements

## References

[1] D.I. Enache, J.K. Edwards, P. Landon, B. Solsona-Espriu, A.F. Carley, A.A. Herzing, M. Watanabe, C.J. Kiely, D.W. Knight, G.J. Hutchings, Science 311 (2006) 362–365.
[2] X.M. Yang, X.N. Wang, J.S. Qiu, Appl. Catal. A: Gen. 382 (2010) 131–137.
[3] T. Harada, S. Ikeda, F. Hashimoto, T. Sakata, K. Ikeue, T. Torimoto, M. Matsumura, Langmuir 26 (2010) 17720–17725.
[4] S. Marx, A. Baiker, J. Phys. Chem. C 113 (2009) 6191–6201.
[5] K. Mori, T. Hara, T. Mizugaki, K. Ebitani, K. Kaneda, J. Am. Chem. Soc. 126 (2004) 10657–10666.
[6] A.S.K. Hashmi, G.J. Hutchings, Angew. Chem. Int. Ed. 45 (2006) 7896–7936.
[7] N. Zheng, G.D. Stucky, Chem. Commun. 37 (2007) 3862–3864.
[8] M. Pagliaro, S. Campestrini, R. Ciriminna, Chem. Soc. Rev. 34 (2005) 837–845.
[9] T. Konda, S. Nishiyama, S. Tsuruya, Phys. Chem. Chem. Phys. 1 (1999) 5393–5399.
[10] M.M. Deng, G.F. Zhao, Q.S. Xue, L. Chen, Y. Lu, Appl. Catal. B: Environ. 99 (2010) 222–228.
[11] X.M. Wang, G.J. Wu, N.J. Guan, L.D. Li, Appl. Catal. B: Environ. 115–116 (2012) 7–15.
[12] N. Dimitratos, J.A. Lopez-Sanchez, D. Morgan, A.F. Carley, R. Tiruvalam, C.J. Kiely, D. Bethell, G.J. Hutchings, Phys. Chem. Chem. Phys. 11 (2009) 5142–5153.
[13] L.C. Wang, Y.M. Liu, M. Chen, Y. Cao, H.Y. He, K.N. Fan, J. Phys. Chem. C 112 (2008) 6981–6987.
[14] C. Keresszegi, D. Ferri, T. Mallat, A. Baiker, J. Phys. Chem. B 109 (2005) 958–967.
[15] D. Ferri, C. Mondelli, F. Krumeich, A. Baiker, J. Phys. Chem. B 110 (2006) 22982–22986.
[16] H.Y. Han, S.J. Zhang, H.W. Hou, Y.T. Fan, Y. Zhu, Eur. J. Inorg. Chem. 8 (2006) 1594–1600.
[17] J. Chen, Q.H. Zhang, Y. Wang, H.L. Wan, Adv. Synth. Catal. 350 (2008) 453–464.
[18] K.-M. Choi, T. Akita, T. Mizugaki, K. Ebitani, K. Kaneda, New J. Chem. 27 (2003) 324–328.
[19] Y.T. Chen, Z. Guo, T. Chen, Y.H. Yang, J. Catal. 275 (2010) 11–24.
[20] Y.T. Chen, H.M. Lim, Q.H. Tang, Y.T. Gao, T. Sun, Q.Y. Yan, Y.H. Yang, Appl. Catal. A: Gen. 380 (2010) 55–65.
[21] S.F.J. Hackett, R.M. Brydson, M.H. Gass, I. Harvey, A.D. Newman, K. Wilson, A.F. Lee, Angew. Chem. Int. Ed. 46 (2007) 8593–8596.
[22] U.R. Pillai, E. Sahle-Demessie, Green Chem. 6 (2004) 161–165.
[23] A.H. Lu, W.C. Li, Z.S. Hou, F. Schuth, Chem. Commun. 10 (2007) 1038–1040.
[24] S.H. Liu, R.F. Lu, S.J. Huang, A.Y. Lo, S.H. Chien, S.B. Liu, Chem. Commun. 32 (2006) 3435–3437.
[25] R. Kou, Y.Y. Shao, D.H. Mei, Z.M. Nie, D.H. Wang, C.M. Wang, V.V. Viswanathan, S. Park, I.A. Aksay, Y.H. Lin, Y. Wang, J. Liu, J. Am. Chem. Soc. 133 (2011) 2541–2547.
[26] J. Luo, Q. Zhang, J. Garcia-Martinez, S.L. Suib, J. Am. Chem. Soc. 130 (2008) 3198–3207.
[27] E.I. Ross-Medgaarden, I.E. Wachs, W.V. Knowles, A. Burrows, C.J. Kiely, M.S. Wong, J. Am. Chem. Soc. 131 (2009) 680–687.
[28] Q.H. Tang, S.Q. Hu, Y.T. Chen, Z. Guo, Y. Hu, Y.A. Chen, Y.H. Yang, Microporous Mesoporous Mater. 132 (2010) 501–509.
[29] G. Ovejero, J.L. Sotelo, M.D. Romero, A. Rodriguez, M.A. Ocana, G. Rodriguez, J. Garcia, Ind. Eng. Chem. Res. 45 (2006) 2206–2212.
[30] M.S. Bakshi, J. Phys. Chem. C 131 (2009) 10921–10928.
[31] T. Teranishi, M. Miyake, Chem. Mater. 10 (1998) 594–600.
[32] A.Y. Stakheev, L.M. Kustov, Appl. Catal. A: Gen. 188 (1999) 3–35.
[33] C. Linsmeier, E. Taglauer, Appl. Catal. A: Gen. 391 (2011) 175–186.
[34] K. Jiratova, J. Mikulova, J. Klempa, T. Grygar, Z. Bastl, F. Kovanda, Appl. Catal. A: Gen. 361 (2009) 106–116.
[35] Z.R. Yue, W. Jiang, L. Wang, S.D. Gardner, C.U. Pittman, Carbon 37 (1999) 1785–1796.
[36] Y.C. Son, V.D. Makwana, A.R. Howell, S.L. Suib, Angew. Chem. Int. Ed. 40 (2001) 4280–4283.
[37] C.M. Zhou, Y.T. Chen, Z. Guo, X. Wang, Y.H. Yang, Chem. Commun. 47 (2011) 7473–7475.
[38] K.Q. Ding, J. Chin. Chem. Soc. 55 (2008) 543–549.
[39] Y.T. Chen, H.J. Zhen, Z. Guo, C.M. Zhou, C. Wang, A. Borgna, Y.H. Yang, J. Catal. 283 (2011) 34–44.
[40] T. Mallat, A. Baiker, Chem. Rev. 104 (2004) 3037–3058.
[41] T. Suzuki, R. Souda, Surf. Sci. 448 (2000) 33–39.
[42] P. Maity, C.S. Gopinath, S. Bhaduri, G.K. Lahiri, Green Chem. 11 (2009) 554–561.
[43] J.D. Grunwaldt, M. Caravati, A. Baiker, Chem. Eur. J. 110 (2006) 25586–25589.
[44] F. Li, Q.H. Zhang, Y. Wang, Appl. Catal. A: Gen. 334 (2008) 217–226.
[45] S.J. Tauster, Acc. Chem. Res. 20 (1987) 389–394.
[46] A. Caballero, J.P. Holgado, V.M. Gonzalez-delaCruz, S.E. Habas, T. Herranz, M. Salmeron, Chem. Commun. 26 (2010) 1097–1099.
[47] A.R. Gandhe, J.S. Rebello, J.L. Figueiredo, J.B. Fernandes, Appl. Catal. B: Environ. 72 (2007) 129–135.
[48] M.C. Alvarez-Galvan, B. Pawelec, V.A.D. O'Shea, J.L.G. Fierro, P.L. Arias, Appl. Catal. B: Environ. 51 (2004) 83–91.
[49] X.F. Tang, Y.G. Li, X.M. Huang, Y.D. Xu, H.Q. Zhu, J.G. Wang, W.J. Shen, Appl. Catal. B: Environ. 62 (2006) 265–273.
[50] C. Keresszegi, D. Ferri, T. Mallat, A. Baiker, J. Catal. 234 (2005) 64–75.